Long-chain Branched Poly(lactic acid)-*b*-poly(lactide-*co*-caprolactone): Structure, Viscoelastic Behavior and Triple Shape Memory Effect as Smart Bone Fixation Material

[1]Yalong Liu, [1]Huijie Cao, [1]Lin Ye, [2]Phil Coates, [2]Fin Caton-Rose, [1]Xiaowen Zhao*

[1]State Key Laboratory of Polymer Materials Engineering, Polymer Research Institute of Sichuan University, Chengdu 610065, China

[2]School of Engineering, Design and Technology, University of Bradford, Bradford, UK

*Corresponding author. Tel.: 862885408802; Fax: 862885402465. E-mail address: zhaoxiaowenscu@126.com

Table of Contents

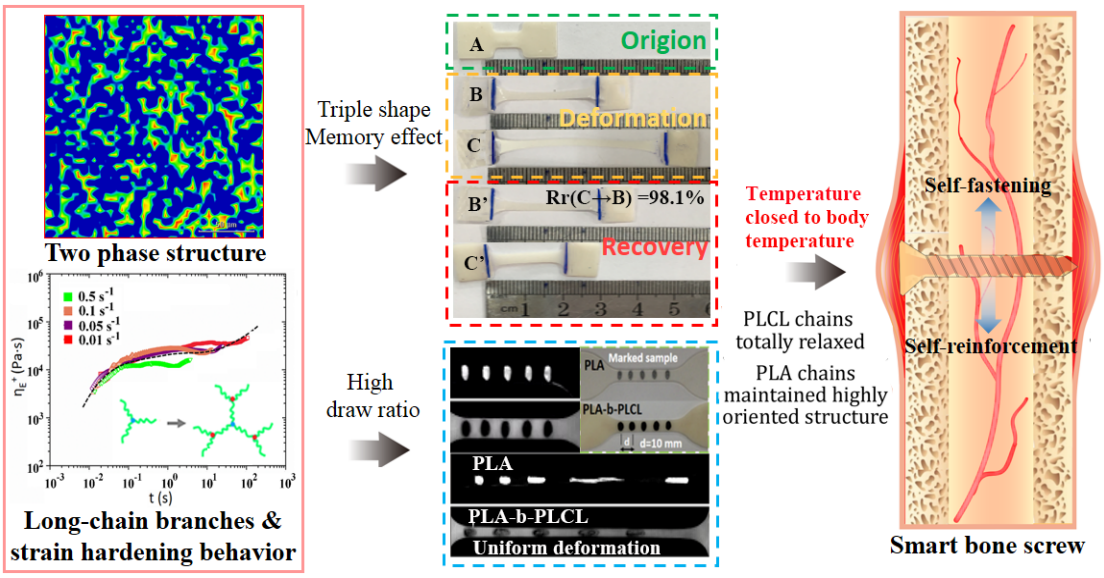

Abstract

A novel fully biosbased poly(lactic acid)-*b*-poly(lactide-*co*-caprolactone) (PLA-*b*-PLCL) with two phase structure and long-chain branches was specifically designed and prepared through reactive melt processing. The results showed that PLCL segments were introduced onto PLA chains successfully. With the increase of PLCL content, the blockier distribution of LA/CL chain sequences of the sample was exhibited. PLA-*b*-PLCL showed two distinct thermal transitions, corresponding to the glass transition of PLA and PLCL domains, respectively, while the phase morphology changed from sea-island to co-continuous structure with increasing PLCL content. Due to the long-chain branched structure, PLA-*b*-PLCL samples showed much high viscoelasticity, strong molecular entanglement and obvious strain-hardening behavior, resulting in high draw ratio of the sample during orientation process, while the tensile strength and the modulus of the oriented sample reached up to 173 MPa and 5.4 GPa respectively, which basically met the requirements of bone screws. Moreover, PLA-*b*-PLCL showed triple shape memory effect at 55 ^{o}C and 120 ^{o}C, respectively. For PLA-b-30wt%PLCL, the recovery ratio can reach up to 98.1% under 55 ^{o}C, while high mechanical properties can be maintained, realizing self-reinforcement and self-fastening effect simultaneously as smart bone fixation material.

Key words: Poly(lactic acid); two phase structure; long-chain branches; viscoelastic behavior; triple shape memory effect

1. Introduction

Poly(lactic acid) (PLA) is a thermoplastic and biodegradable aliphatic polyester derived from naturally occurring organic acid (lactic acid).[1-3] Due to the excellent biocompatibility, complete biodegradability and non-toxic nature of degradation products, PLA has been demonstrated to be a suitable material for producing bone

fixation devices such as absorbable plates and screws.[4-8] Unfortunately, just as most biodegradable polymers, some properties of PLA are unsatisfactory when it acts as implanted bone fixation materials: the mechanical strength of PLA is not sufficient for fixation of weight loading bones; self-fastening property is deficient compared with some shape memory alloys.[9]

Molecular orientation can enhance the mechanical properties of PLA significantly.[10] Singh et al.[11] fabricated orientated PLA-based nanocomposite through solid-state drawing. The tensile strength as high as 71 MPa and modulus of 1.72 GPa were obtained for the oriented sample. Yuan et al.[12] produced PLLA fibers through melt extrusion and hot drawing. The maximum draw ratio reached up to 589% and the tensile modulus of the fiber was 3.6~5.4 GPa. However, due to the linear structure and narrow molecular weight distribution, PLA exhibited very low viscosity and poor melt elasticity. Therefore, ultra-drawing and high orientation of PLA is very difficult, resulting in a limited enhancement of the mechanical property through molecular orientation. In our previous study, long-chain branched PLA (LCB-PLA) was prepared through reactive melt processing. Due to the enhanced entanglement between long-branched chains, LCB-PLA showed obvious enhanced melt viscoelasticity compared with neat PLA, and thus high draw ratio as high as 1200% can be obtained during solid phase hot drawing.

As a kind of semi-crystalline polymer, the crystalline domains and molecular entanglement of PLA and LCB-PLA can serve as the fixed phase, while their amorphous domains acts as the reversible phase to realize thermally induced shape memory effect to a certain extent.[13-16] However, the glass transition temperature (T_g) of both neat PLA and LCB-PLA was about 65 ℃. Therefore, samples could hardly recover their shape under low temperature, especially like body temperature [17], and

then self-fastening function cannot be achieved when used as implant bone fixation screw.[18-20]

In this work, by means of molecular design, biodegradable poly(lactide-co-caprolactone) (PLCL), with much lower T_g (-20~30 ℃) than that of PLA, was selected as another component of PLA system to construct two-phase separated structure, and thus owing to the two transition temperature of the material, triple shape memory effect was expected to be achieved for PLA system.[21-22] Meanwhile, in order to improve the viscoelasticity and thus obtain high draw ratio during solid phase hot drawing, the block copolymer of PLA-*b*-PLCL with long-chain branched structure was prepared through reactive melt processing. Consequently, on one hand, highly oriented PLA-*b*-PLCL with excellent mechanical properties can be obtained by solid hot drawing. On the other hand, when such highly oriented PLA-*b*-PLCL was heated to temperature range between transition temperature of PLA and PLCL, the PLCL domains relaxed, while PLA domains maintained the orientation structure, resulting in a partial shape recovery of the sample, which was beneficial for PLA based material to realize controllable shape recovery and self-fastening as well as self-reinforcement effect as smart bone fixation material.

2. Experimental

2.1. Materials

Poly(lactic acid) (PLA) (3052D) in pellet form was purchased from Nature Works Co., USA. Poly(lactide-*co*-caprolactone) (PLCL), pyromellitic dianhydride (PMDA) and pentaerythritol polyglycidyl ether (PGE) were all commercial grade products.

2.2. Materials preparation

2.2.1 Preparation of PLA-*b*-PLCL

PLA-*b*-PLCL with long-chain branches was prepared through reactive processing.

PLA with different content of PLCL were mixed in Haake internal melt mixer (Rhecocrd 90, Germany) at 180 ℃. After the pellets were melted, 2 wt% PMDA and 2 wt% PGE were added into the mixer to react with PLA and PLCL. After reaction for 10~30 min, the product was removed from the mixer and cut into small granules.

2.2.2 Orientation of PLA-*b*-PLCL

The orientation of PLA-*b*-PLCL samples was conducted via solid phase hot drawing by using a 5567 material testing machine from Instron Co. (U.S.A). The original length of the samples between clamps was 10 mm, and a constant deformation rate of 50 mm/min was applied. The orientation temperature was in the range of 70~120 ℃.

2.3. Measurements

The structure of PLA samples was analyzed with a Nicolet-560 Fourier transform infrared spectrometer (FTIR) (U.S.) and an AV HD 400 NMR spectrometer (Bruker Co, Germany). The fractured surface morphology of PLA samples was observed with a JEOL JSM-5900LV scanning electron microscope (SEM, JEOL Co, Japan). Raman imaging measurements were carried out with DXRxi Raman Imaging Microscope (Thermo Fisher, USA). The mapping was conducted over an area of 200μm × 200μm. Thermo mechanical properties of the PLA samples were obtained by a dynamic mechanical analyzer (Netzsch DMA 242C). The viscoelasticity property of PLA samples was analyzed with an AR 1500ex dynamic stress rheometer (TA Instruments, USA). The elongational viscosity of PLA samples was measured by an ARES reheometer (TA instrument) at 170 ℃. The tensile strength of PLA samples was measured with a 5567 material testing machine (Instron Co, USA).

3. Result and discussions

3.1. Structure characterization of PLA-*b*-PLCL with long-chain branches

The block copolymer of PLA-*b*-PLCL with long-chain branched structure was prepared through a two-step ring-opening reaction with anhydride and epoxy during processing as shown in Figure 1. BOB model [23] was applied to investigate the chain structures of PLA-*b*-PLCL, which indicated that the topological structure of the sample was made of linear chains, star-like chains with three arms and tree-like chains with two generations.

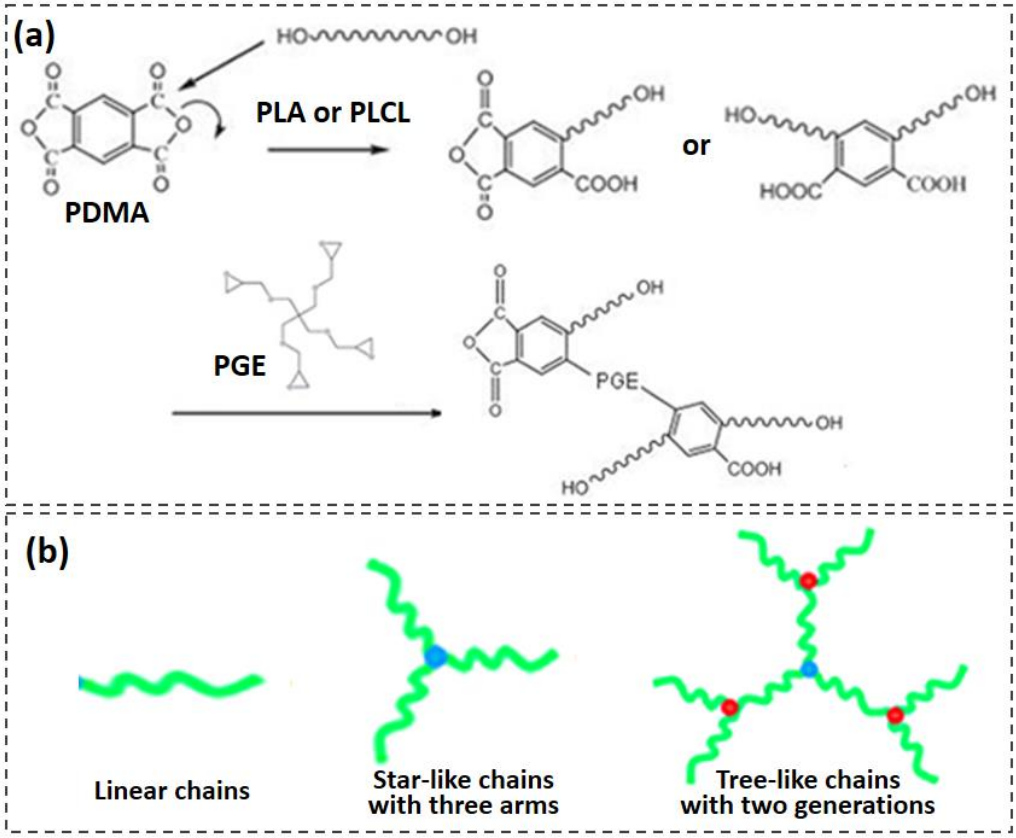

Figure 1. Chain extension reactions (a) and possible chain structures of PLA-*b*-PLCL (b)

3.1.1 Molecular structure

The FTIR spectra of neat PLA and purified PLA-*b*-PLCL samples with varying PLCL content were depicted in Figure 2. For neat PLA, the absorption peaks at 2998 cm^{-1} and 2944 cm^{-1} were assigned to the stretching vibration of C–H bond of methyl and methylene groups, respectively. The absorption peaks at 1453 cm^{-1} and 1352 cm^{-1} were attributed to the flexural vibration of C–H bond of methyl and methylene groups. A single absorption peak at 1756 cm^{-1} can be observed corresponding to the stretching

vibration of C=O bond. In addition, absorption peaks in the region of 1000~1150 cm^{-1} was assigned to the stretching vibrations of C–O–C bond of ester group. For PLA-*b*-PLCL samples, besides absorption peaks attributed to PLA, two new absorption peaks at 1732 cm^{-1} and 1184 cm^{-1} were observed, which was assigned to the vibration of C=O and C–O–C bond of ester group in PLCL block connected directly with long alkyl chain.[24,25] With the increase of PLCL component, the intensity of these two peaks increased, indicating that more and more PLCL molecules were introduced onto PLA chains.

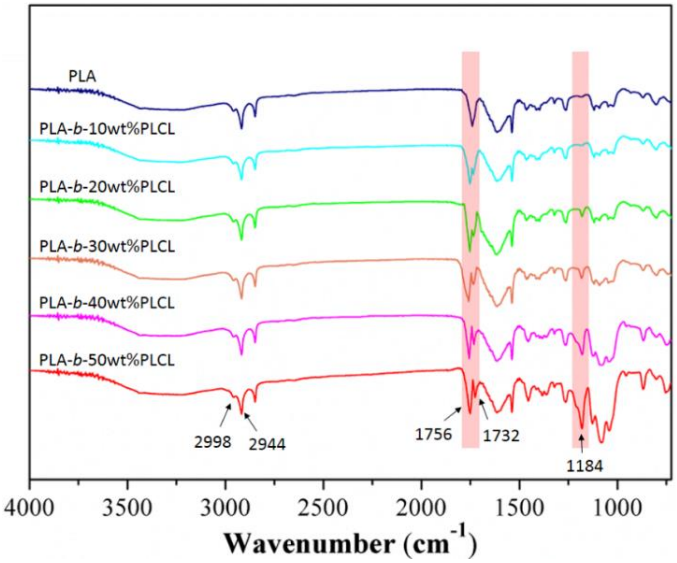

Figure 2. FTIR spectra of neat PLA and PLA-*b*-PLCL samples

^{13}C NMR was used to further confirm the chain structure of PLA-*b*-PLCL. As shown in Figure 3a, three identifiable peaks can be observed for neat PLA. The peak at δ16.62 ppm belonged to the methyl carbons (–CH_3) of PLA, while the peak at δ68.99 ppmδ169.58 ppm was the typical chemical shifts for the methine carbon (–CH–) and carbonyl carbon (–COO–), respectively. Because the chain of both PLCL and PLA-*b*-PLCL were composed of ε-caprolactone (CL) segment and lactide (LA) segment, some new signals can be observed for these samples in the ^{13}C NMR spectrum. The resonance at δ173.2 ppm belonged to the carbonyl carbon of CL segment and the peak at δ63.2 ppm was assigned to methine carbon of LA segment

which connected directly with CL units. A series of signals in the region of δ24.0~25.8 ppm were the chemical shifts of the β and γ-methylene carbon atoms of CL units,[26] and the detailed peaks in this region for PLA-*b*-PLCL samples with different PLCL content were shown in Figure 3b. It can be observed that, the intensity of CL–CL–CL, LA–CL–CL, CL–CL–LA and LA–CL–LA triads signals increased with the increase of PLCL content, indicating that more PLA molecules were connected with PLCL chains.

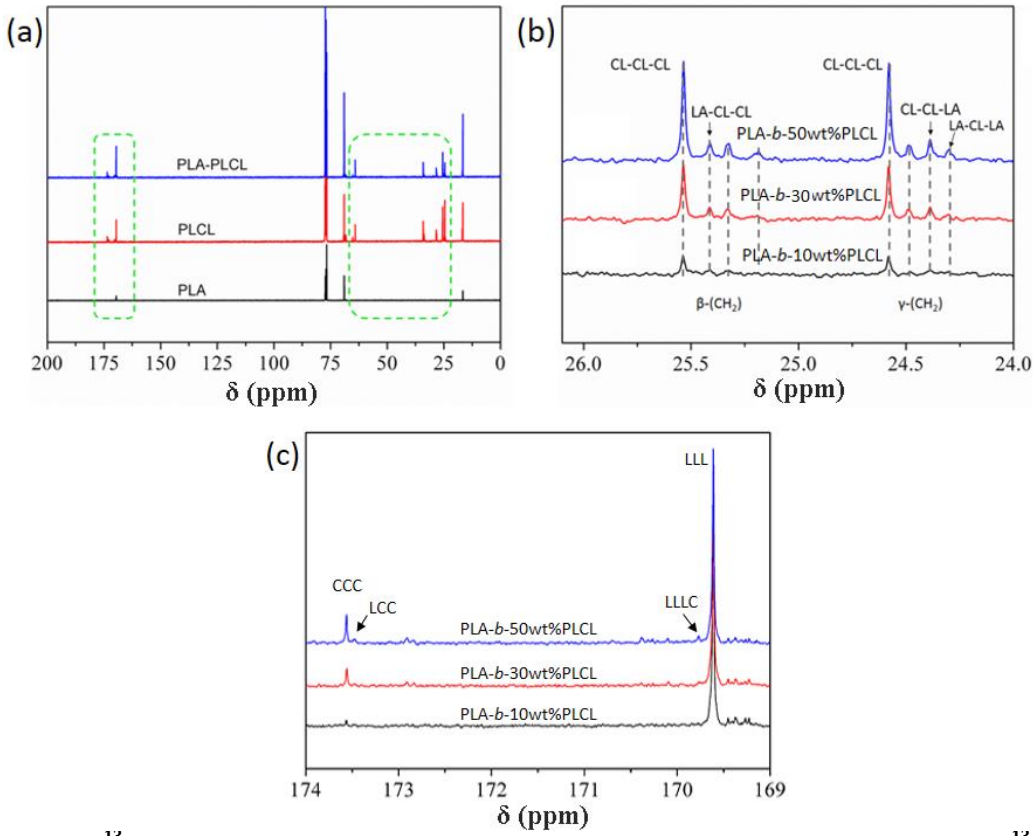

Figure 3. ^{13}C NMR spectrum of neat PLA, neat PLCL and PLA-*b*-PLCL samples (a); ^{13}C NMR spectrum of PLA-*b*-PLCL in the region of δ24.0~26.0 ppm (b); ^{13}C NMR spectrum of PLA-*b*-PLCL in the region of δ169.0~174.0 ppm (c)

As shown in Figure 3c, the average lengths of lactide blocks (L_{LA}) and ε-caprolactone blocks (L_{CL}) can be calculated based on the intensities of the carbonyl signals in the region of δ169.0~174.0 ppm:[27]

$$L_{CL} = \frac{I_{CCC}}{I_{LCC}} + 1 \quad (1)$$

$$L_{LA} = \frac{I_{LLL}}{I_{LLLC}} + 1 \quad (2)$$

where I_{CCC} and I_{LLL} were the intensities of ε-caprolactone–ε-caprolactone and $_{L}$-lactide–$_{L}$-lactide triads, respectively; I_{LCC} and I_{LLLC} represented the intensities of ε-caprolactone–$_{L}$-lactide triad and tetrad, respectively.

For the PLA-*b*-10wt%PLCL sample, the values of L_{LA} and L_{CL} were 56.7 and 2.8 respectively. With the increase of PLCL content, more PLCL molecules were introduced onto the PLA chains, and the values of L_{LA} decreased to 30 for PLA-*b*-30wt%PLCL and further decreased to 16.6 for PLA-*b*-50wt%PLCL, while the values of L_{CL} almost maintained constant, indicating blockier distribution of chain sequences of the sample.

3.1.2 Two phase structure

Figure 4 showed the temperature dependence of storage modulus and tan delta (tanδ) of the samples. It can be obviously seen that the storage modulus curves of neat PLA presented a single transition step at about 60~70 ℃, corresponding to the glass transition of PLA. However, all PLA-*b*-PLCL samples exhibited two well-separated thermal transition steps in the range of -20~0 ℃ and 60~70 ℃, corresponding to dramatic drop in storage modulus curves. The higher one (60~70 ℃) was attributed to the glass transition of PLA phase, and the lower one (-20~0 ℃) was attributed to the glass transition of PLCL phase. In Figure 4b, two distinct thermal transitions of PLA-*b*-PLCL samples can be also observed clearly in the tanδ curve. Such two distinct thermal transitions to switch off/on the molecular mobility may enable PLA-*b*-PLCL to memory two temporary shapes when stimulated by heat.

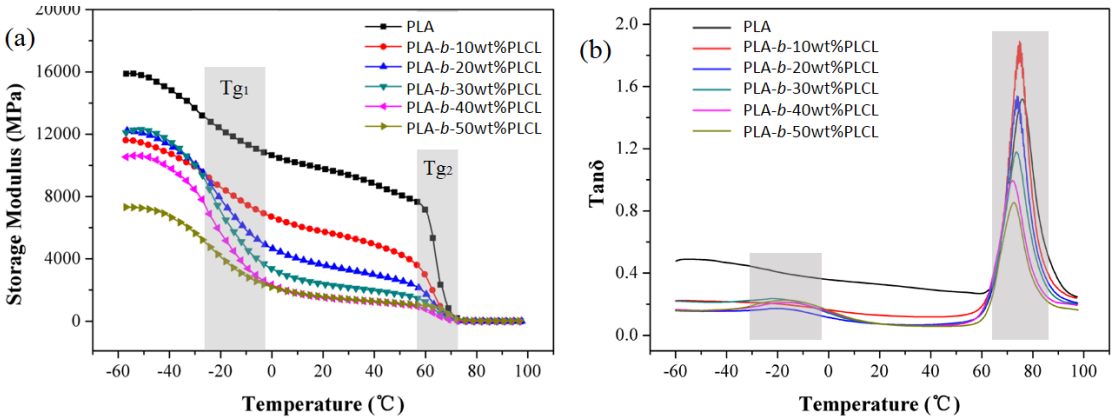

Figure 4. Dynamic mechanical behaviors of neat PLA and PLA-*b*-PLCL samples

Figure 5 showed the SEM micrographs of cryogenic fracture surfaces for neat PLA and PLA-*b*-PLCL samples. It was found that neat PLA showed a featureless morphology, while for the PLA-*b*-PLCL, a micro-phase separated morphology was observed. For PLA-*b*-10wt%PLCL, droplets of PLCL component with size range of 0.1~1μm dispersed uniformly in PLA matrix. When the content of PLCL rose to 20wt%, the sample still showed distinct sea-island structure, while the size of the dispersed PLCL domains became larger. When the content of PLCL was higher than 30wt%, both PLA and PLCL components formed the continuous phase and a well-defined co-continuous structure was built up.

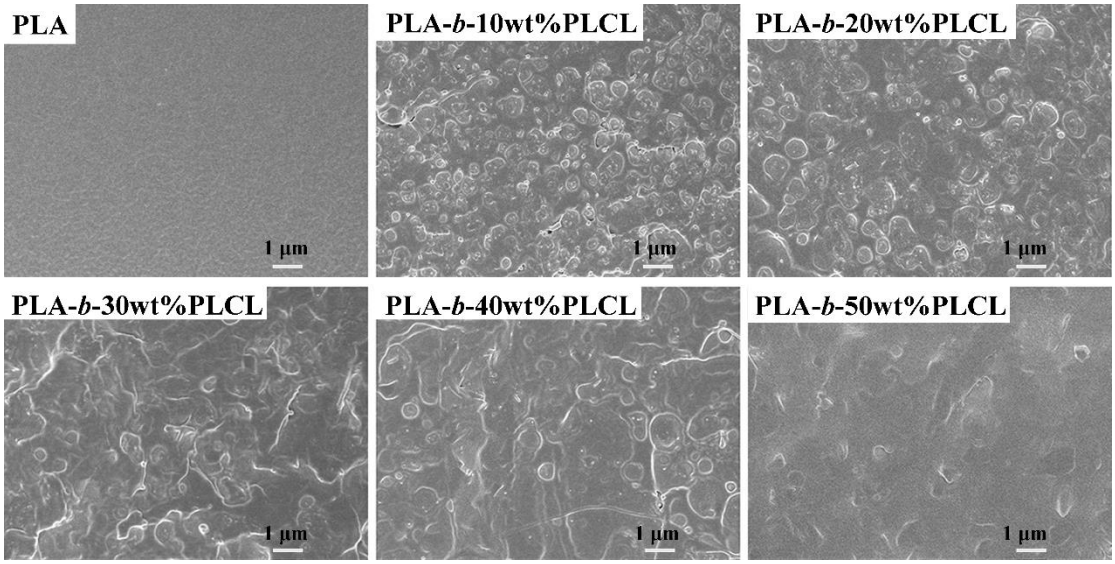

Figure 5. SEM micrographs of cryogenic fracture surfaces for neat PLA and PLA-*b*-PLCL samples (magnification: 10000×)

In order to further understand the distribution of the two components in

PLA-*b*-PLCL samples, Raman mapping was performed. Specific Raman spectra of neat PLA and PLCL in association with various band assignments were shown in Figure 6a. At a glance of the whole Raman spectra, the two samples showed very similar absorption peaks. However, different from neat PLA, the C=O stretching band centered at 1728cm $^{-1}$ was a distinct feature for PLCL domains, and thus this band was chosen to distinguish PLCL from PLA during mapping analysis.[28,29] PLCL domains were denoted in the mapping images as green colors as shown in Figure 6(b~f). For PLA-*b*-PLCL samples with PLCL content of 10wt% and 20wt%, the mapping images showed well-separated PLA and PLCL phases, and PLCL phase was confined as small domains between PLA phases. For samples with PLCL content higher than 30wt%, continuous phase structure can be observed, confirming the morphology observed by SEM.

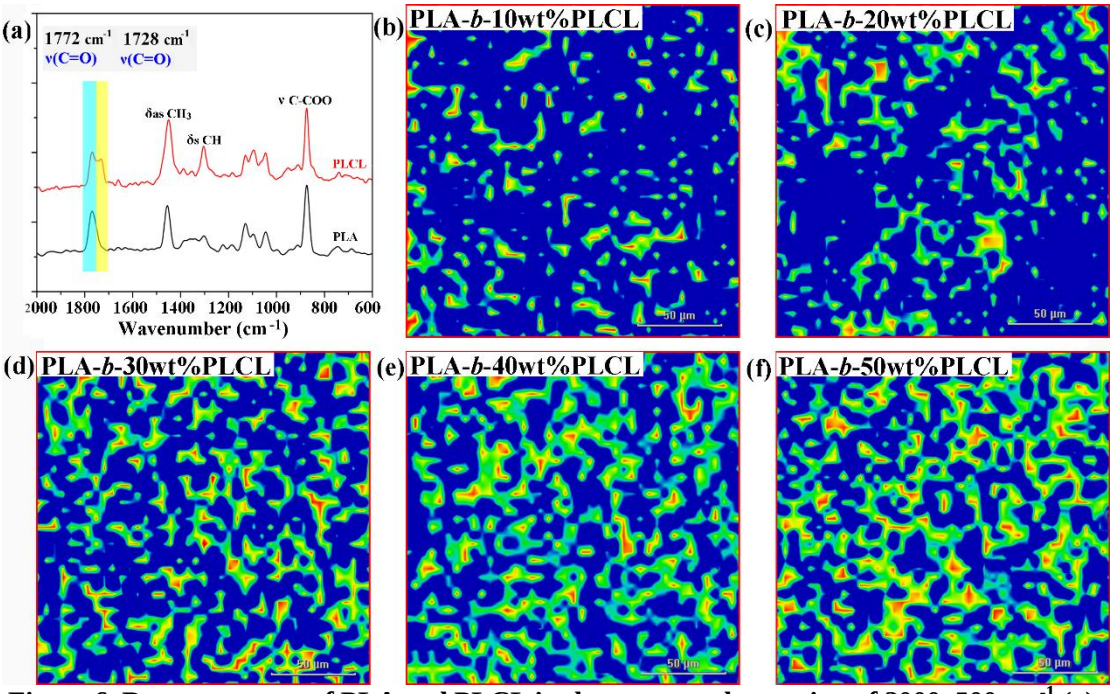

Figure 6. Raman spectra of PLA and PLCL in the wavenumber region of 2000~500 cm^{-1} (a); Raman mapping images of PLA-*b*-PLCL samples (b~f)

3.2 Viscoelastic behaviour and molecular entanglements of PLA-*b*-PLCL with long-chain branches

3.2.1 Viscoelastic behaviour

The complex viscosity of PLA-*b*-PLCL samples as a function of frequency was plotted in Figure 7a. For neat PLA, the complex viscosity remained constant in low frequency region, and then decreased at higher frequency, showing a transition from the Newtonian plateau to the power-law regime. For PLA-*b*-PLCL samples, higher complex viscosities than that of neat PLA in full frequency range can be observed, and with the increase of PLCL content, the onset of the shear thinning regimes started at a lower frequency. When PLCL content was higher than 20wt%, the Newtonian plateau almost disappeared.

The storage modulus, G′, and loss modulus, G″, of PLA-*b*-PLCL samples were shown in Figure 7(b-c). It was noted that, all samples showed almost identical G′ and G″ values at high frequencies, and with the decrease of frequency, both G′ and G″ decreased. In the terminal region, the G′ and G″ of neat PLA followed the well-known frequency dependences of linear polymer, that was, $G' \propto \omega^2$ and $G'' \propto \omega$, for which only the longest relaxation times contributed to the viscoelastic behavior.[30] Therefore, for neat PLA, in the log-log plot of G′ and G″ with frequency, slopes of 2 and 1 can be respectively observed in this region. Compared with neat PLA, PLA-*b*-PLCL samples showed much higher G′ values in terminal region and the terminal slopes decreased obviously. Such deviation from the curve of linear PLA at low frequency indicated high elasticity for PLA-*b*-PLCL samples due to the existence of long-chain branched structure with much longer relaxation time than that of the linear ones.

The Cole-Cole plot of PLA-*b*-PLCL samples were shown in Figure 7d,[31] which exhibited the relationship between real viscosity (η′) and imaginary viscosity (η″). It was found that, the Cole-Cole plot for neat PLA was arc-shaped. However, for PLA-*b*-PLCL samples, the radius of the arc became larger, and showed evident

upturning at high viscosities, which was also observed by others for polymers with long-chain branches. Moreover, with the increase of PLCL content, the upturning became more and more evident.

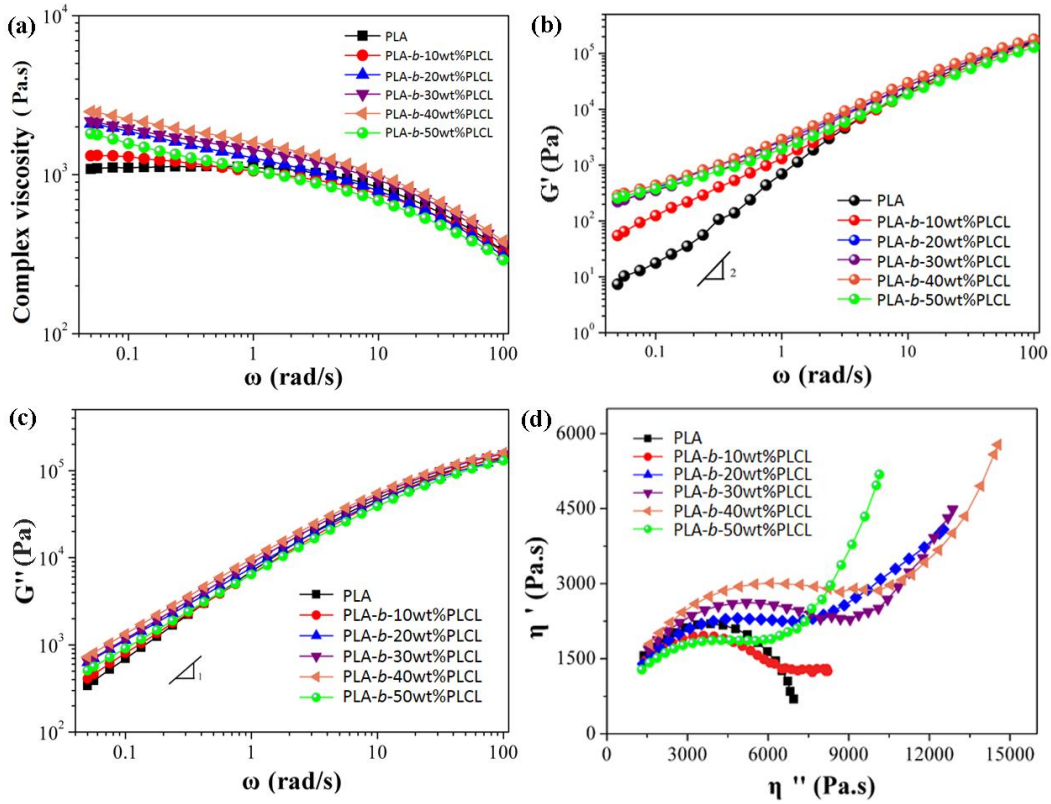

Figure 7. The complex viscosity (a), storage modulus (b), loss modulus (c) and Cole-Cole curves (d) of neat PLA and PLA-*b*-PLCL samples obtained by dynamic frequency sweep at 180 ℃

3.2.2 Molecular entanglements

Entanglements between PLA molecules are essential in understanding its rheological properties. The average entanglement density (υ_e) can be obtained with the equation:[32]

$$\upsilon_e = \rho_a / M_e \quad (3)$$

where ρ_a and *Me* are the density and the average molar mass between adjacent entanglement points, respectively.

The entanglement molar mass (M_e) of PLA-b-PLCL can be calculated based on the plateau modulus G_N^0: [33,34]

$$Me = \frac{4\rho RT}{5G_N^0} \quad (4)$$

where ρ is the density; T and R are the absolute temperature and gas constant, respectively. Based on the crossover modulus *Gx* (*Gx*= *G′*= *G″*), a semi-quantitative method was applied to extract the value of G_N^0 [32]:

$$\log\left(\frac{G_N^0}{G_X}\right) = 0.38 + \frac{2.63\log(M_w/M_n)}{1+2.45\log(M_w/M_n)} \quad (5)$$

where *Mw* and *Mn* are weight-average molecular weight and number-average molecular weight of PLA-b-PLCL samples, respectively.

The Arabic numbers 1 and 2 were used to represent the components PLA and PLCL, respectively, and then there were three types of possible entanglements: 1–1, 2–2 and 1–2 (assumed to be equal to 2–1). M_{e12} was defined as the average entanglement molar mass between PLCL and PLA chains (dissimilar chains), which can be obtained with the equation:

$$Me_{12} = 2\varphi_1\varphi_2 RT(\rho_1\rho_2)^{\frac{1}{2}}/(G_N^0 - \varphi_1^2 G_{N1}^0 - \varphi_2^2 G_{N2}^0) \quad (6)$$

where φ_1 and φ_2 are the volume fraction of PLA and PLCL, respectively; ρ_1 and ρ_2 are the density of neat PLA and neat PLCL, respectively; G_N^0, G_{N1}^0 and G_{N2}^0 are the plateau modulus of PLA-b-PLCL, neat PLA and neat PLCL, respectively.

The entanglement state can be compared through the value of M_e and M_{e12}. As shown in Figure 8, the values of M_{e12} were smaller than M_e for samples with PLCL content of 30%~50%, indicating that the dissimilar chains were more likely to entangle with each other than similar ones. Moreover, the υ_e values increased with increasing PLCL content.

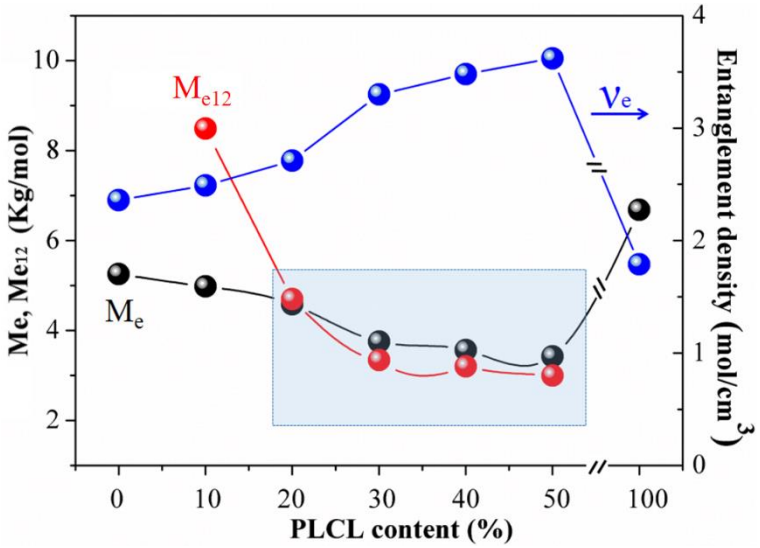

Figure 8. Average entanglement molar mass and entanglement density of neat PLA and PLA-*b*-PLCL samples

3.2.3 Elongational viscosity

Uniaxial viscosity of neat PLA and PLA-*b*-PLCL samples was shown in Figure 9(a~f). The elongational viscosities of the neat PLA increased with time at the start of stretching, and then decreased, showing strain-softening phenomena. In contrast, the PLA-*b*-PLCL samples displayed strain-hardening behavior,[31,35] which was represented as a sudden increase of the viscosity at high strain. Moreover, the strain hardening behavior became more and more obvious with the increase of PLCL content. Such strain-hardening behavior was important for solid hot drawing processing where high melt strength was required.

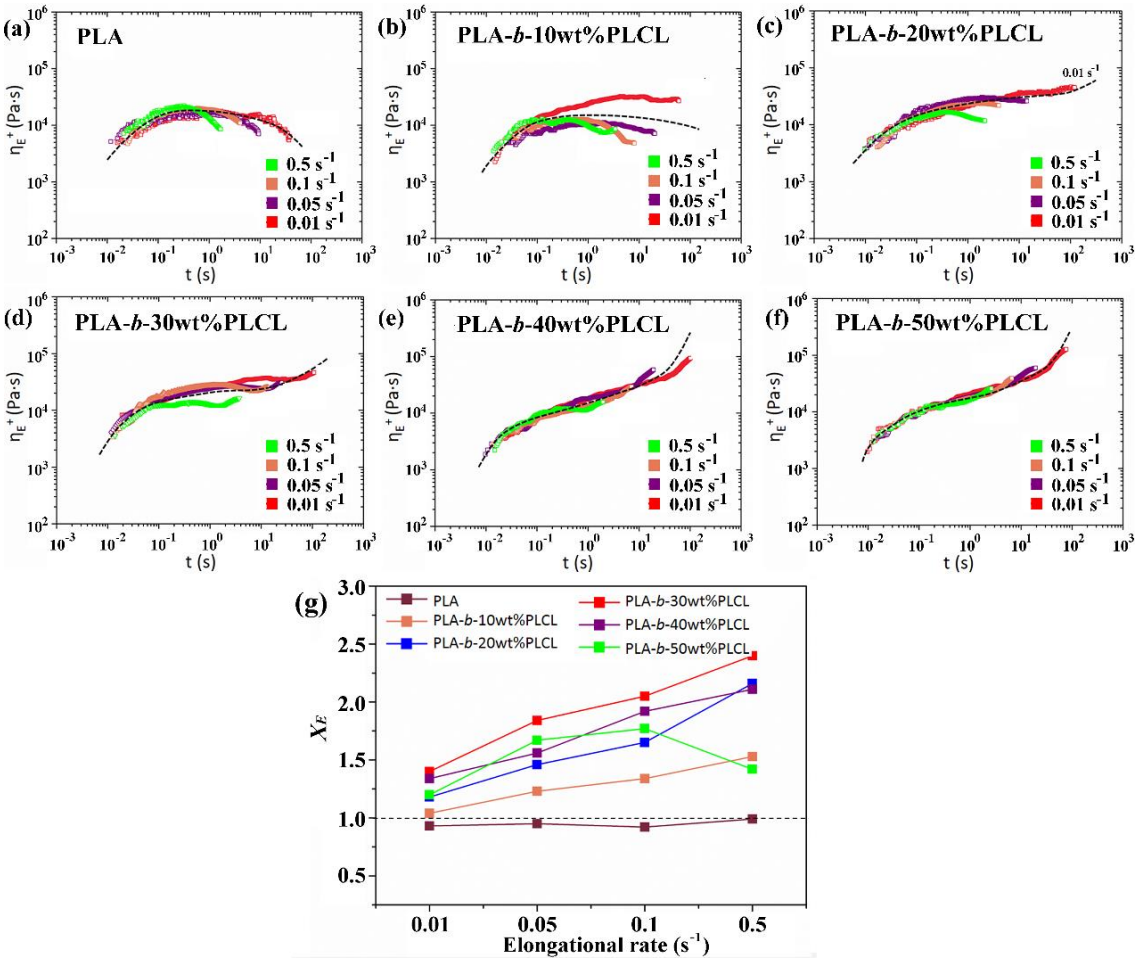

Figure 9. Elongational viscosity (a~f) and strain-hardening coefficient (g) of neat PLA and PLA-*b*-PLCL samples

The strain-hardening coefficient, $X_{E,}$ was calculated to quantitatively evaluate the strain-hardening behavior of PLA-*b*-PLCL:

$$X_E = \eta_E^+(t, \varepsilon_0)/3\eta^+(t) \quad (6)$$

where η_E^+ was the elongational viscosity of material at Hencky strain of 2.7 and η^+ was transient shear viscosity in the linear viscoelasticity region.

As shown in Figure 9(g), the strain-hardening coefficient was always below 1 for neat PLA, implying the obviously strain softening behavior. For PLA-*b*-PLCL samples, the strain-hardening coefficient increased with increasing strain rate, indicating that entanglements between branched chains can improve the stretching ability of the backbone.

3.3 Orientation of PLA-*b*-PLCL and its triple shape memory effect

3.3.1 Orientation

The successful formation of long-chain branched structure and obvious improvement of viscoelasticity encouraged us to perform solid phase hot drawing on PLA-*b*-PLCL samples. The maximum draw ratio of PLA-*b*-PLCL with varing PLCL content was shown in Figure 10a. For neat PLA, the maximum draw ratio was about 500%, while for PLA-*b*-PLCL samples, with the increase of PLCL content, the draw ratio increased initially and then declined somewhat. The maximum draw ratio reached up to 960% for PLA-*b*-30wt%PLCL.

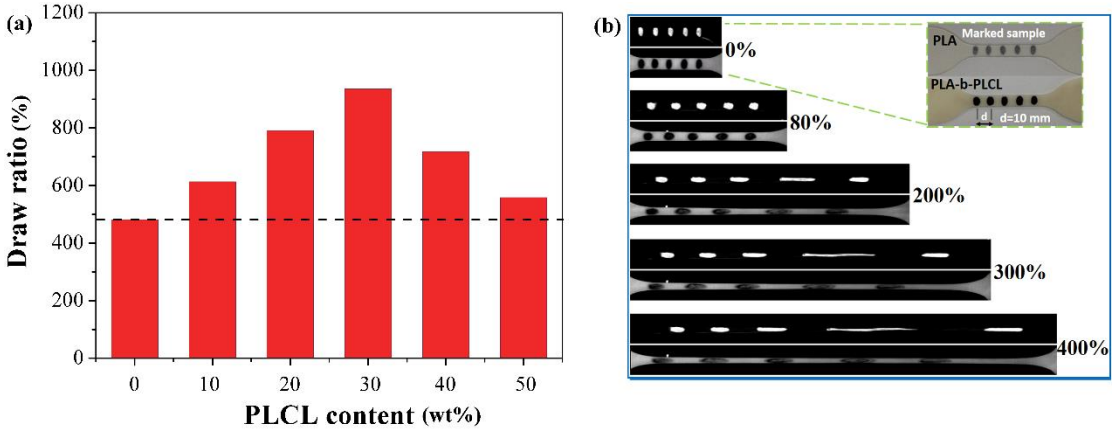

Figure 10. Maximum draw ratio of neat PLA and PLA-*b*-PLCL samples at 80 ℃ (a); Real-time photographs of neat PLA and PLA-*b*-30wt%PLCL during drawing process at 80 ℃ (b)

The real-time photographs of neat PLA and PLA-*b*-30wt%PLCL samples during stretching at 80 ℃ were shown in Figure 10b. A series of black dot markers were printed on the front flat face of the sample. Through the observation of the deformation of the dots during drawing, the deformation of the sample can be evaluated. For neat PLA, dots on the sample were elongated uneven, suggesting an inhomogeneous deformation occurred during drawing. However, for PLA-*b*-PLCL sample, dots were elongated uniformly with almost equal length, indicating that the sample was homogeneous stretched.

For PLA-*b*-30wt%PLCL sample with draw ratio of 900%, the tensile strength reached up to 173 MPa, and the modulus was about 5.4 GPa, which basically met the

requirements for bone fixation materials, realizing efficient self-reinforcement for PLA.

3.3.2 Triple shape memory effect

In order to investigate the triple shape memory effect of PLA-*b*-PLCL, the original shape A of the sample was deformed at 80 ℃ and fixed at 50 ℃ to yield the first temporary shape B, which was further deformed at 50 ℃ and fixed at -10 ℃ to yield the second temporary shape C (as shown in Figure 11). During the deformation process, for neat PLA and PLA-*b*-50wt%PLCL, the second temporary shape C cannot be obtained due to the fracture of the sample. Meanwhile, PLA-*b*-PLCL samples with PLCL content of 10~40wt% can be deformed to shape C, and the shape fixity ratio (R_f) were all higher than 94%. Upon reheating to 55 ℃, due to the relaxation of PLCL chains to a higher entropy state [36,37], the second temporary shape C was recovered to shape B′ which was quite similar with shape B. The shape recovery ratio (R_r) of the samples were listed in Tab.1. For PLA-*b*-30wt%PLCL, the R_r(C→B) can reach up to 98.1%, and after recovery, the tensile strength and modulus of the sample were maintained as high as 124 MPa and 3.7 GPa, respectively. Then, samples were further heated to 120 ℃, and the original shape A was partly recovered, suggesting that PLA-*b*-PLCL possessed the capability to memorize multiple shapes at different transition temperatures.

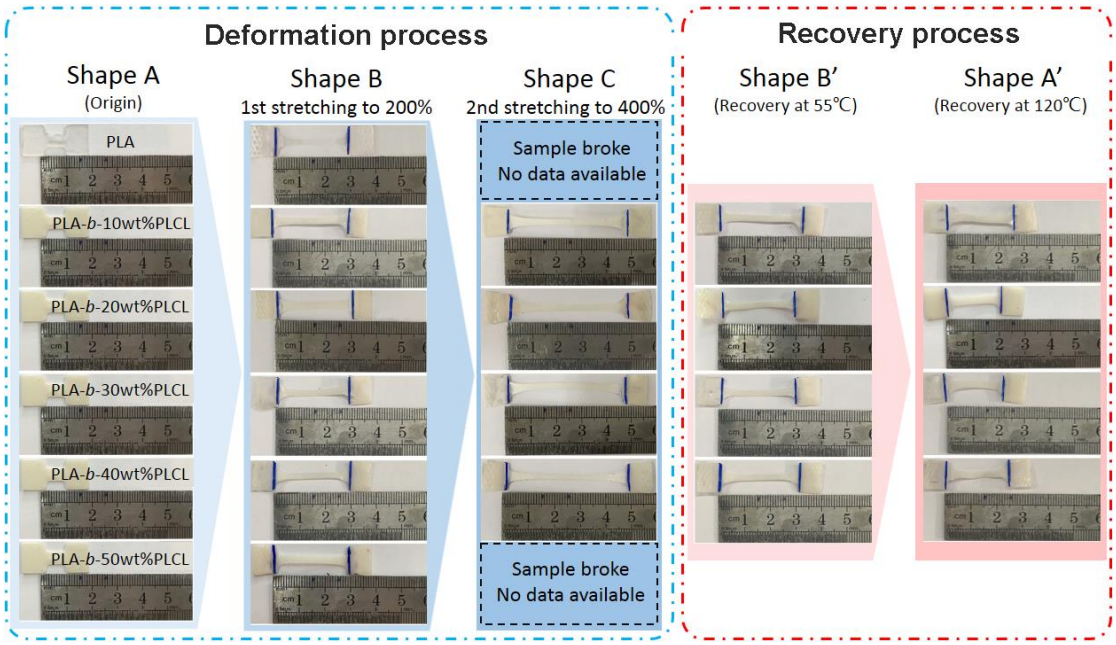

Figure 11. Triple shape memory process of neat PLA and PLA-*b*-PLCL samples

Table 1. Shape fixity ratio and shape recovery ratio of neat PLA and PLA-*b*-PLCL samples

Sample	R_f(A→B) [%]	R_f(B→C) [%]	R_r(C→B) [%]	R_r(B→A) [%]
Neat PLA	96.6 ±1.1	-	-	-
PLA-*b*-10wt%PLCL	97.8 ±1.5	95.4 ±2.1	92.5 ±1.4	40.5 ±2.7
PLA-*b*-20wt%PLCL	98.2 ±1.7	95.2 ±2.5	97.7 ±2.2	51.3 ±2.5
PLA-*b*-30wt%PLCL	97.6 ±2.3	94.2 ±1.9	98.1 ±2.0	50.6 ±2.5
PLA-*b*-40wt%PLCL	98.4 ±1.2	95.3 ±2.2	95.4 ±1.9	42.6 ±2.6
PLA-*b*-50wt%PLCL	97.3 ±2.5	-	-	-

Figure 12 showed the potential application of PLA-*b*-PLCL as smart bone fixation material. During bone fixation surgery, highly oriented PLA-*b*-PLCL screw, which possessed smaller diameter than that of the screw hole, was very convenient for implantation. And then, when such screw was heated to 55 ℃ which was close to the human body temperature, shape recovery process completed within 30s, far less than the exposure time (about 100s) [38] that can cause burns for human tissue under 55 ^{o}C, resulting in the shrinkage along longitudinal direction and enlargement of the transverse section of the screw. Therefore, the gap between screw and the hole was healed, and the screw was stabilized and fastened in surrounding tissues (Figure 12c).

Moreover, after such recovery the sample still possessed excellent mechanical properties, due to the high orientation structure maintained in PLA domains, realizing self-reinforcement and self-fastening effect simultaneously as bone screw.

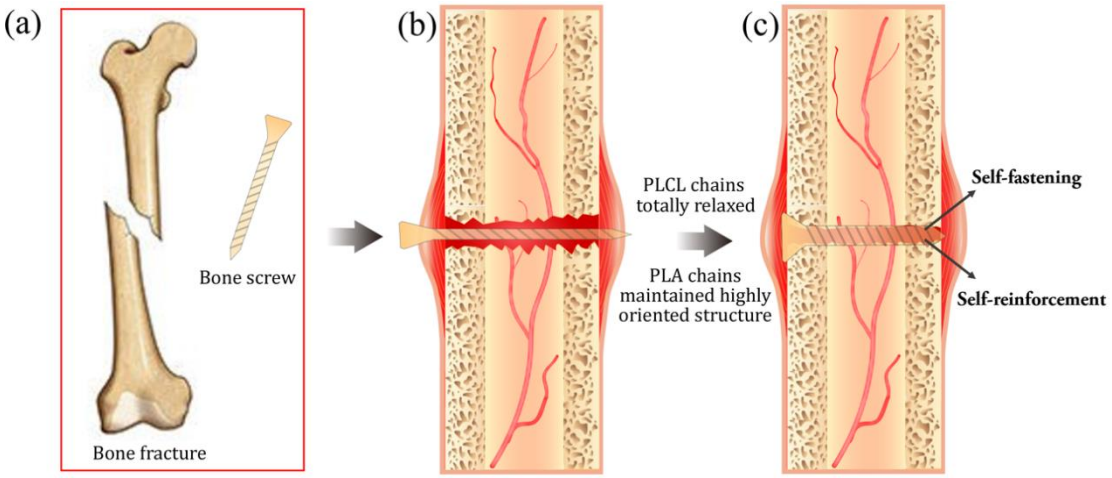

Figure 12. Schematic illustration of the application of highly oriented PLA-*b*-PLCL as bone screw

4. Conclusion

Poly(lactic acid)-*b*-poly(lactide-*co*-caprolactone) (PLA-*b*-PLCL) with two phase structure and long-chain branches was prepared through reactive melt processing. The FTIR and ^{13}C NMR analysis confirmed that PLCL chains were grafted onto PLA. With increasing PLCL content, the average lengths of LA segment decreased while the length of CL segment almost maintained constant, indicating blockier distribution of chain sequences of the sample. The DMA indicated that PLA-*b*-PLCL exhibited two distinct thermal transitions corresponding to the glass transition of PLA and PLCL, respectively. The phase morphology of PLA-*b*-PLCL samples changed from sea-island structure to co-continuous structure with the increase of PLCL content. Due to long chain branching, compared with neat PLA, PLA-*b*-PLCL samples showed much higher complex viscosity, storage modulus and loss modulus. Moreover, for PLA-*b*-PLCL, the Cole-Cole curve showed an evident upturning at high viscosities. Owing to the enhanced molecular entanglement, PLA-*b*-PLCL samples displayed obvious strain hardening behavior, and thus higher draw ratio could be achieved

during orientation process. The tensile strength reached up to 173 MPa, and the modulus was about 5.4 GPa for PLA-*b*-30wt%PLCL sample with draw ratio of 900%, which basically met the requirements of bone fixation materials. PLA-*b*-PLCL possessed the capability to memorize multiple shapes at different transition temperatures. For PLA-*b*-30wt%PLCL, the recovery ratio can reach up to 98.1% under 55^{o}C, and after recovery the sample could maintain excellent mechanical properties. The present work showed promising potential for developing PLA bone fixation medical materials with excellent self-reinforcing and self-fastening properties.

Acknowledgements

This work was supported by National Natural Science Foundation of China (Grant No. 51773122) and State Key Laboratory of Polymer Materials Engineering (Grant No. sklpme2019-2-21).

References

(1) Billimoria, K.; Heeley, E. L.; Parsons, N. An investigation into the crystalline morphology transitions in poly-L-lactic acid (PLLA) under uniaxial deformation in the quasi-solid-state regime. *Eur. Polym. J.* **2018**, *101*, 127-139.

(2) Zhang, H.; Bai, H.; Deng, S.; Fu, Q. Achieving all-polylactide fibers with significantly enhanced heat resistance and tensile strength via in situ formation of nanofibrilized stereocomplex polylactide. *Polymer* **2019**, *166*, 13-20.

(3) Jing, Z.; Shi, X.; Gu, J. W. Synthesis and properties of poly (lactide)/poly (ε-caprolactone) multiblock supramolecular polymers bonded by the self-complementary quadruple hydrogen bonding. *Polymer* **2017**, *121*, 124-136.

(4) Nair, L. S.; Laurencin, C. T. Biodegradable polymers as biomaterials. *Prog. Polym. Sci.* **2007**, *32*, 762-798.

(5) Lasprilla, A. J. R.; Martinez, G. A. R.; Lunelli, B. H. Poly-lactic acid synthesis for application in biomedical devices-a review. *Biotechnol. Adv.* **2012**, *30*, 321-328.

(6) Rasal, R. M.; Janorkar, A. V.; Hirt, D. E. Poly(lactic acid) modifications. *Prog. Polym. Sci.* **2010**, *35*, 338-356.

(7) Santos, T. K.; Merlini, C.; Aragones, Á. Manufacturing and characterization of plates for fracture fixation of bone with biocomposites of poly(lactic acid-co-glycolic acid) (PLGA) with calcium phosphates bioceramics. *Mat. Sci. Eng. C-Mater.* **2019**, *103*, 109728.

(8) Wei, Y.; Huang, R.; Dong, P.; Fu, Q. Preparation of polylactide/poly (ether) urethane blends with excellent electro-actuated shape memory via incorporating carbon black and carbon nanotubes hybrids fillers. Chinese. *J. Polym. Sci.* **2018**, *36*, 1175-1186.

(9) Li, J.; Zhao, X.; Ye, L. Multiple shape memory behavior of highly oriented long-chain-branched poly(lactic acid) and its recovery mechanism. *J. Biomed. Mater. Res. A* **2019**, *107*, 872-883.

(10) Grijpma, D. W.; Altpeter, H.; Bevis, M. J. Improvement of the mechanical properties of poly(D, L-lactide) by orientation. *Polym. Int.* **2002**, *51*, 845-851.

(11) Singh, A.; Wei, J.; Herrera, N. Synergistic effect of chitin nanocrystals and orientations induced by solid-state drawing on PLA-based nanocomposite tapes. *Compos. Sci. Technol.* **2018**, *162*, 140-145.

(12) Yuan, X.; Mak, A.T.; Kwok, K. W. Characterization of poly(L-lactic acid) fibers produced by melt spinning. *J. Appl. Polym. Sci.* **2001**, *81*, 251-260.

(13) Sun, L.; Huang, W. M. Mechanisms of the multi-shape memory effect and temperature memory effect in shape memory polymers. *Soft Matter* **2010**, *6*, 4403-4406.

(14) Merlettini, A.; Gigli, M.; Ramella, M. Thermal annealing to modulate the shape memory behavior of a biobased and biocompatible triblock copolymer scaffold in the human body temperature range. *Biomacromolecules* **2017**, *18*, 2499-2508.

(15) Samuel, C.; Barrau, S.; Lefebvre, J. M. Designing multiple-shape memory polymers with miscible polymer blends: evidence and origins of a triple-shape memory effect for miscible PLLA/PMMA blends. *Macromolecules* **2014**, *47*, 6791-6803.

(16) Guo, B.; Chen, Y.; Lei, Y. Biobased poly(propylene sebacate) as shape memory polymer with tunable switching temperature for potential biomedical applications. *Biomacromolecules* **2011**, *12*, 1312-1321.

(17) Deng, Z.; Guo, Y.; Zhao, X.; Guo, B. Stretchable degradable and electroactive shape memory copolymers with tunable recovery temperature enhance myogenic differentiation. *Acta Biomater.* **2016**, *46*, 234-244.

(18) Wang, W.; Ping, P.; Chen, X. Polylactide-based polyurethane and its shape-memory behavior. *Eur. Polym. J.* **2006**, *42*, 1240-1249.

(19) Fan, X.; Tan, B. H.; Li, Z. Control of PLA stereoisomers-based polyurethane elastomers as highly efficient shape memory materials. *ACS Sustain. Chem. Eng.* **2016**, *5*, 1217-1227.

(20) Gu, L.; Cui, B.; Wu, Q. Y. Bio-based polyurethanes with shape memory behavior at body temperature: Effect of different chain extenders. *RSC Adv.* **2016**, *6*, 17888-17895.

(21) Zhao, X.; Dong, R.; Guo, B. Dopamine-incorporated dual bioactive electroactive

shape memory polyurethane elastomers with physiological shape recovery temperature, high stretchability, and enhanced C2C12 myogenic differentiation. *ACS Appl. Mater. Inter*. **2017**, *9*, 29595-29611.

(22) Zhao, Q.; Qi, H. J.; Xie, T. Recent progress in shape memory polymer: New behavior, enabling materials, and mechanistic understanding. *Prog*. *Polym*. *Sci*. **2015**, *49*, 79-120.

(23) Li, Z. Q.; Liu, L. Structure and antimicrobial properties of long-chain branched poly (lactic acid). *J. Biomed. Mater. Res. A* **2019**, *107*, 2458-2467.

(24) Kalpan, G.; Shalini, V. S.; Jonnalagadda, S. Fast degradable poly(L-lactide-co-e-caprolactone) microspheres for tissue engineering: synthesis, characterization, and degradation behavior. *J*. *Polym*. *Sci*. *Pol*. *Chem*. **2007**, *45*, 2755-2764.

(25) Zhang, H.; Lou, S.; Williams, G. R. A systematic study of captopril-loaded polyester fiber mats prepared by electrospinning. *Int*. *J*. *Pharmaceut*. **2012**, *439*, 100-108.

(26) Fernández, J.; Etxeberria, A.; Ugartemendia, J. M. Effects of chain microstructures on mechanical behavior and aging of a poly(L-lactide-co-ε-caprolactone) biomedical thermoplastic-elastomer. *J*. *Mech*. *Biomed*. **2012**, *12*, 29-38.

(27) Lipik, V. T.; Kong, J. F.; Chattopadhyay, S. Thermoplastic biodegradable elastomers based on ε-caprolactone and l-lactide block co-polymers: A new synthetic approach. *Acta Biomater*. **2010**, *6*, 4261-4270.

(28) Luckachan, G. E.; Mittal, V. Evaluation of crystallinity variation and phase dispersion in polymer blends and nanocomposites by Raman mapping. *J*. *Polym*. *Res*. **2015**, *22*, 237.

(29) Peponi, L.; Sessini, V.; Arrieta, M. P. Thermally-activated shape memory effect on biodegradable nanocomposites based on PLA/PCL blend reinforced with hydroxyapatite. *Polym*. *Degrad*. *Stabil*. **2018**, *151*, 36-51.

(30) Chen, C. Q.; Ke, D. M.; Zheng, T. T. An ultraviolet-induced reactive extrusion to control chain scission and long-chain branching reactions of polylactide. *Ind*. *Eng*.

Chem. *Res*. **2016**, *55*, 597-605.

(31) Xu, H.; Fang, H.; Bai, J. Preparation and characterization of high-melt-strength polylactide with long-chain branched structure through γ-radiation-induced chemical reactions. *Ind*. *Eng*. *Chem*. *Res*. **2014**, *53*, 1150-1159.

(32) Wu, S. Chain entanglement and melt viscosity of compatible polymer blends: poly(methyl methacrylate) and poly(styrene-acrylonitrile). *Polymer* **1987**, *28*, 1144-1148.

(33) Graessley, W. W. Some phenomenological consequences of the Doi-Edwards theory of viscoelasticity. Journal of Polymer Science: *J*. *Polym*. *Sci*. *Polym*. *Phys*. *Ed*. **1980**, *18*, 27-34.

(34) Fetters, L. J.; Lohse, D. J.; Richter, D. Connection between polymer molecular weight, density, chain dimensions, and melt viscoelastic properties. Macromolecules **1994**, 27, 4639-4647.

(35) Gu, L.; Xu, Y.; Fahnhorst, G. W. Star vs long chain branching of poly(lactic acid) with multifunctional aziridine. J. Rheol. **2017**, 61, 785-796.

(36) Li, M.; Chen, J.; Shi, M.; Guo, B. Electroactive anti-oxidant polyurethane elastomers with shape memory property as non-adherent wound dressing to enhance wound healing. Chem. Eng. J. **2019**, 375, 121999.

(37) Wu, Y.; Wang, L.; Zhao, X.; Guo, B. Self-healing supramolecular bioelastomers with shape memory property as a multifunctional platform for biomedical applications via modular assembly. Biomaterials **2016**, 104, 18-31.

(38) Bull, J. P.; Lawrence, J. C. Thermal conditions to produce skin burns. Fire Mater. **1979**, 3, 100-105.

Table caption

Table 1. Shape fixity ratio and shape recovery ratio of neat PLA and PLA-*b*-PLCL samples

Figure captions

Figure 1. Chain extension reactions (a) and possible chain structures of PLA-b-PLCL (b)

Figure 2. FTIR spectra of neat PLA and PLA-*b*-PLCL samples

Figure 3. ^{13}C NMR spectrum of neat PLA, PLCL and PLA-*b*-PLCL samples (a); ^{13}C NMR spectrum in the region of δ24.0~26.0 ppm (b); ^{13}C NMR spectrum in the region of δ169.0~174.0 ppm (c)

Figure 3. ^{13}C NMR spectrum of neat PLA, neat PLCL and PLA-*b*-PLCL samples (a); ^{13}C NMR spectrum of PLA-*b*-PLCL in the region of δ24.0~26.0 ppm (b); ^{13}C NMR spectrum of PLA-*b*-PLCL in the region of δ169.0~174.0 ppm (c)

Figure 4. Dynamic mechanical behaviors of neat PLA and PLA-*b*-PLCL samples

Figure 5. SEM micrographs of cryogenic fracture surfaces for neat PLA and PLA-*b*-PLCL samples (magnification: 10000×)

Figure 6. Raman spectra of PLA and PLCL in the wavenumber region of 2000~500 cm^{-1} (a); Raman mapping images of PLA-*b*-PLCL samples (b~f)

Figure 7. The complex viscosity (a), storage modulus (b), loss modulus (c) and Cole-Cole curves (d) of neat PLA and PLA-*b*-PLCL samples obtained by dynamic frequency sweep at 180 ℃

Figure 8. Average entanglement molar mass and entanglement density of neat PLA and PLA-*b*-PLCL samples

Figure 9. Elongational viscosity (a~f) and strain-hardening coefficient (g) of neat PLA and PLA-*b*-PLCL samples

Figure 10. Maximum draw ratio of neat PLA and PLA-*b*-PLCL samples at 80 ℃ (a); Real-time photographs of neat PLA and PLA-*b*-30wt%PLCL during drawing process at 80 ℃ (b)

Figure 11. Triple shape memory process of neat PLA and PLA-*b*-PLCL samples

Figure 12. Schematic illustration of the application of highly oriented PLA-*b*-PLCL as bone screw